

Equilibrium and nonequilibrium properties of systems with long-range interactions

Stefano Ruffo^{1,2}

¹ Dipartimento di Energetica “S. Stecco” and CSDC, Università di Firenze via s. Marta 3, I-50139 FIRENZE, Italy

² INFN, Sezione di Firenze

Received: date / Revised version: date

Abstract. We briefly review some equilibrium and nonequilibrium properties of systems with long-range interactions. Such systems, which are characterized by a potential that weakly decays at large distances, have striking properties at equilibrium, like negative specific heat in the microcanonical ensemble, temperature jumps at first order phase transitions, broken ergodicity. Here, we mainly restrict our analysis to mean-field models, where particles globally interact with the same strength. We show that relaxation to equilibrium proceeds through quasi-stationary states whose duration increases with system size. We propose a theoretical explanation, based on Lynden-Bell’s entropy, of this intriguing relaxation process. This allows to address problems related to nonequilibrium using an extension of standard equilibrium statistical mechanics. We discuss in some detail the example of the dynamics of the free electron laser, where the existence and features of quasi-stationary states is likely to be tested experimentally in the future. We conclude with some perspectives to study open problems and to find applications of these ideas to dipolar media.

PACS. 05.20.-y Classical statistical mechanics – 05.70.Fh Phase transitions:general studies – 05.45.-a Nonlinear dynamics and chaos

1 Introduction

For systems with long-range interaction the pair potential decays at large distances with a weak power law $V(r) \sim r^{-s}$, with $s \leq d$, the space dimension [1]. Examples are: gravity, whose statistical mechanics is made more complex by the unremovable *singularity* of the potential at the origin; Coulomb interactions, with the phenomenon of *charge screening* which allows the treatment of globally neutral systems; dipolar media, that display the well known feature of *shape dependence*; vortices interacting with logarithmic potential in $d = 2$, for which Onsager first discussed microcanonical features, like the presence of *negative temperatures*, at the first Statphys meeting in Florence [2].

Long-range interactions can be made extensive, but are intrinsically non-additive. Let us consider the simplest model of ferromagnetic systems, the Curie-Weiss mean-field Hamiltonian

$$H = -\frac{J}{2N} \sum_{i,j} \sigma_i \sigma_j \quad (1)$$

in which the spins $\sigma_i = \pm 1$ are globally coupled with strength $J > 0$. The energy scales with system size, $H \sim N$, and an intensive energy density $\mathcal{E} = \lim_{N \rightarrow \infty} H/N$ can be defined in the thermodynamic limit, but, due to the

presence of N^2 links, the sum of the energies of two subsystems I and II is never giving the total energy $E_{I+II} \neq E_I + E_{II}$. Besides that, for mean-field models of this kind the set of accessible macrostates in the space of intensive parameters E and $M = \sum_i \sigma_i$, can be *non convex* (see Fig. 1). These two mathematical properties, that can be present only at finite N for short-range interactions ($s > d$), have important physical consequences. The specific heat [3], and other quantities related to the curvature of the entropy, like susceptibility [4], can become negative in certain energy ranges; jumps in temperature can be realized at first-order microcanonical transitions [5]; broken ergodicity can be present both for finite N and in the thermodynamic limit [6] (see Sect. 5). All this is inscribed inside the general framework of *ensemble inequivalence* [7,8]. We will briefly illustrate these features for a mean-field XY model with two-spin and four-spin interactions in Sect. 2.

All the above is for equilibrium properties (i.e. maximal entropy states), but systems with long-range interactions also show a very slow approach to equilibrium. For systems with short-range interactions it has been definitely assessed that, appropriately selecting the initial state, the subsequent relaxation to equilibrium takes place on a finite time in the thermodynamic limit [9]. On the contrary, since the seminal paper of Lynden-Bell [3], it has been proposed that systems with long-range interac-

tions can display a two-step relaxation. In a first stage, the system relaxes rapidly (“violently”, according to Lynden-Bell) to a *quasi-stationary* state whose lifetime increases with system size: two types of dependencies have been proposed, either power-law N^δ [10] or logarithmic $\ln N$ [6], depending on some detailed property of the initial state. In a second stage, the system begins a slow approach to equilibrium that may be either direct or proceed through successive relaxations to different quasi-stationary states. The fact that the lifetime of quasi-stationary states diverges with system size allows to obtain a separation of the two time scales. This scenario, originally proposed for gravity, has been extended to the two-dimensional Euler equation, the original Onsager’s system, by Chavanis [11]. A theoretical proposal has been advanced by Lynden-Bell in order to interpret the initial relaxation to a quasi-stationary state: that the system tries to maximize an entropy which takes into account additional “constraints” appearing in the thermodynamic limit, the most relevant of those being the normalization of the one-body distribution function [3]. Although the initial numerical tests of this theory gave some hope of success [12], its predictions were subsequently disproved for several systems, even for the simple one-dimensional self-gravitating system [13] and the theory fell into some discredit. We will show in Sect. 3 results for the so-called Hamiltonian Mean Field (HMF) model [14] (a mean-field XY model) for which Lynden-Bell theory has a straightforward application and leads to predictions that are in reasonable agreement with numerical simulations [16]. A recent domain of application of Lynden-Bell’s ideas is to the free electron laser [15], where this approach allows to predict the features of the intensity saturation of the laser, simply knowing the initial conditions, without explicitly solving the equations of motion, as was typically done before: in a sense, this constitutes the statistical mechanics of the free electron laser. This application is likely to produce in the future experimental tests of the features of quasi-stationary states, as we discuss in Sect. 6.

Furthermore, the macrostates that maximize Lynden-Bell’s entropy for a given energy depend on the initial magnetization of the HMF model. The system undergoes a nonequilibrium phase transition that can be of the second or the first order, and hence a *nonequilibrium tricritical point* is present (see Sect. 4). It is interesting that the concepts of equilibrium phase transition can be extended to states that are not in equilibrium. It means that one can assume *mixing* limited to the phase-space visited by the trajectories on a time scale that is small with respect to the relaxation time to equilibrium.

Sect. 7 is devoted to some final remarks and perspectives of applications to wave-particle systems and to dipolar media.

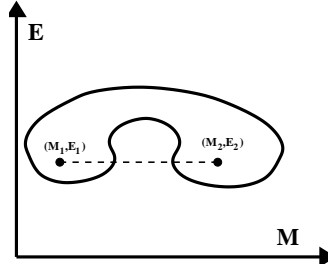


Fig. 1. The set of accessible macrostates in the (E, M) space can have a non-convex shape for systems with long-range interactions, such that if (E_1, M_1) and (E_2, M_2) can be realized macroscopically, this is not necessarily true for all the states joining these two along the straight dashed line.

2 Phase diagram of a mean-field XY model

Let us consider the following Hamiltonian

$$H_{XY} = \sum_{i=1}^N \frac{p_i^2}{2} - \frac{J}{2N} \left(\sum_{i=1}^N \mathbf{s}_i \right)^2 - \frac{K}{4N^3} \left[\left(\sum_{i=1}^N \mathbf{s}_i \right)^2 \right]^2, \quad (2)$$

which can be thought as representing a system of N spins $\mathbf{s}_i = (\cos \theta_i, \sin \theta_i)$ with all-to-all two-spin, J , and four-spin, K , interactions. A kinetic energy term is added, considering p_i as canonically conjugate to θ_i . Because of this addition, Hamiltonian (2) can also represent a system of unit mass particles moving on a circle without collisions, interacting only through a mean-field type potential. This model can be solved in both the canonical and the microcanonical ensemble [17]. The resulting phase diagram is shown in Fig. 2. For both ensembles a tricritical point is present, but its location is different in the two ensembles. The behavior of the order parameter $m = \lim_{N \rightarrow \infty} |\sum_i \mathbf{s}_i|/N$ in the two ensembles is also shown, in order to highlight the striking difference in the predictions. The so-called *caloric curve* (kinetic temperature vs. energy density \mathcal{E}) is reported in Fig. 3. The microcanonical ensemble (full line) predicts a region of negative specific heat, where kinetic temperature T decreases as the energy density is increased. Moreover, a temperature jump is present at the transition energy.

3 Quasi-stationary states

Hamiltonian (2) reduces, for $K = 0$ and adding a constant to shift the energy of the ground state to zero, to that of the HMF model [14]

$$H_{HMF} = \sum_{i=1}^N \frac{p_i^2}{2} + \frac{1}{2N} \sum_{i,j=1}^N (1 - \cos(\theta_i - \theta_j)), \quad (3)$$

whose equilibrium properties are standard: the system undergoes a mean-field second order phase transition in both the microcanonical and the canonical ensemble at the energy $\mathcal{E} = 3/4$, corresponding to the temperature $T = 1/2$ (see [18] for a comprehensive recent review of the model).

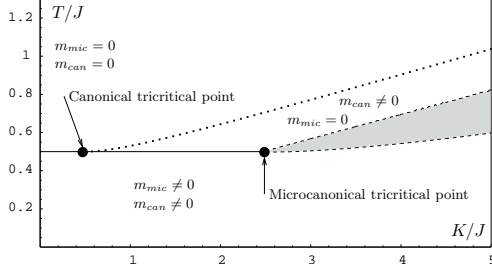


Fig. 2. Phase diagram of Hamiltonian (2). The canonical second order transition line (full horizontal line starting at $T/J = 1/2$) becomes first order (dotted line) at the canonical tricritical point. The microcanonical second order transition line coincides with the canonical one up to $K/J = 1/2$ but it extends further towards the microcanonical tricritical point, located at $K/J = 5/2$. At this latter point, the transition line bifurcates in two first order microcanonical lines (dashed), corresponding to a temperature jump. There are no microcanonical macrostates for parameter values within the shaded region.

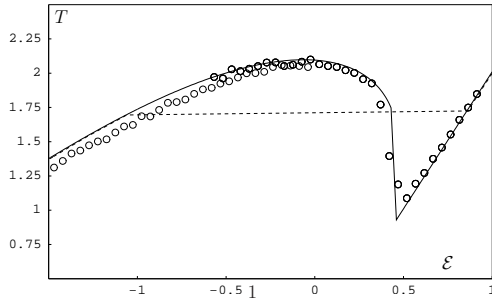


Fig. 3. Caloric curve for $K/J = 10$. The full line is the theoretical prediction in the microcanonical ensemble. The dashed line represents the first order phase transition in the canonical ensemble. The points are obtained from a molecular dynamics simulation of Hamiltonian (2) with $N = 100$.

In order to study nonequilibrium properties, it has been customary to prepare an initial state of the “water-bag” type where all the particles are uniformly distributed in a rectangular domain of width $2\Delta\theta$ and height $2\Delta p$ centered around the origin in the single-particle phase space (θ, p) . Once the size of the domain is given, energy and magnetization are uniquely determined: $m_0 = \sin \Delta\theta / \Delta\theta$, $\mathcal{E} = (\Delta p)^2/6 + (1 - m_0^2)/2$. During microcanonical time evolution, energy and total momentum $\sum_i p_i$ remain constant, but magnetization varies, and one expects that it reaches the equilibrium value compatible with the given energy. This is not what happens, as shown in Fig. 4. One observes an initial “violent” relaxation to a plateau value (closer and closer to $m = 0$ as the number of particles is increased), corresponding to the quasi-stationary state, followed by a second relaxation to equilibrium, which takes place on longer and longer times as N increases. The lifetime of the quasi-stationary state has been fitted with a power-law $N^{1.7}$ in Ref. [10].

How does one explain such a behaviour? It is crucial to realize that the mean-field dynamics (3) is well represented

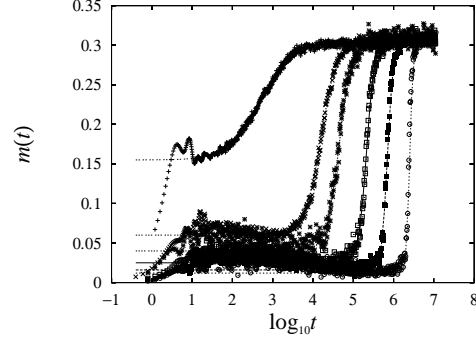


Fig. 4. Magnetization m vs. time t for the HMF model with energy $\mathcal{E} = 0.69$, vanishing total momentum and “water-bag” initial condition with $m_0 = 0$ ($\Delta\theta = \pi$). The value of N increases from left to right: $N = 10^2, 10^3, 2 \times 10^3, 5 \times 10^3, 10^4, 2 \times 10^4$.

in the large N limit by the following Vlasov equation [19]

$$\frac{\partial f}{\partial t} + p \frac{\partial f}{\partial \theta} - \frac{dV}{d\theta} \frac{\partial f}{\partial p} = 0, \quad (4)$$

where $f(\theta, p, t)$ is the single-particle distribution function and the potential $V(\theta)$ is given by

$$\begin{aligned} V(\theta)[f] &= 1 - m_x[f] \cos(\theta) - m_y[f] \sin(\theta), \\ m_x[f] &= \int f(\theta, p, t) \cos \theta d\theta dp, \\ m_y[f] &= \int f(\theta, p, t) \sin \theta d\theta dp. \end{aligned}$$

Besides energy, Vlasov equation also conserves the norm of the distribution function $\int f(\theta, p, t) d\theta dp = 1$, which for the “water-bag” initial condition we have considered implies that the distribution function remains two-level ($0, f_0 = 1/(4\Delta\theta\Delta p)$) at all times. To take this into account, Lynden-Bell has proposed [3] that the system adapts itself on macrostates that maximize the following “fermionic” entropy

$$s_{LB}(\bar{f}) = - \int dp d\theta \left[\frac{\bar{f}}{f_0} \ln \frac{\bar{f}}{f_0} + \left(1 - \frac{\bar{f}}{f_0} \right) \ln \left(1 - \frac{\bar{f}}{f_0} \right) \right], \quad (5)$$

where \bar{f} is the coarse-grained distribution function. The Pauli principle that is implicit in this approach refers to the fact that a “fluid element” in the (θ, p) μ -space cannot occupy a cell which is already occupied by another fluid element, just because the distribution must remain two-level in the course of time. It turns out that the maximization of $s_{LB}(\bar{f})$ at fixed energy, momentum and norm can be explicitly performed for the HMF model, giving the following solution

$$\bar{f}_{QSS}(\theta, p) = \frac{f_0}{e^{\beta(p^2/2 - m[\bar{f}_{QSS}] \cos \theta) + \lambda p + \alpha} + 1}, \quad (6)$$

where β , λ and α are Lagrange multipliers corresponding to the conservation of energy, momentum and norm. As it is clear from equation (6), the quasi-stationary distribution has to be determined self-consistently, since it

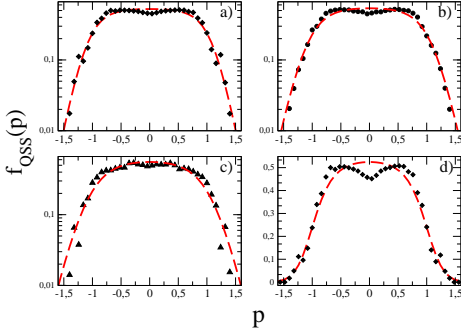


Fig. 5. (color online) Comparison of the theoretical predictions for the quasi-stationary momentum distribution (dashed line) with the numerical simulations (points) performed using Hamiltonian (3) for $\mathcal{E} = 0.69$ and $m_0 = 0.3$ (a), $m_0 = 0.5$ (b), $m_0 = 0.7$ (c). The case $m_0 = 0.3$ is also shown in lin-lin scale in panel (d). For all these cases $m[f_{QSS}] = 0$ (homogeneous quasi-stationary states).

depends on the distribution itself through the magnetization $m[f_{QSS}]$. We have chosen the subscript QSS to mean quasi-stationary-state, because we propose [16] that the states that maximize Lynden-Bell entropy are indeed the quasi-stationary states observed, e.g., in the numerical simulation reported in Fig. 4. The magnetization in the QSS, $m[f_{QSS}] = m_{QSS}$, and the values of the Lagrange multipliers are obtained by solving numerically a set of implicit equations [16], once the energy \mathcal{E} and the initial magnetization m_0 are given (or alternatively $(\Delta\theta, \Delta p)$). Since we look for solutions whose total momentum vanishes, $\lambda = 0$. In Fig. 5 we show the comparison of the predictions of the theory concerning momentum distributions with the numerical simulations performed integrating the equations of motion given by Hamiltonian (3) with $N = 10000$. The agreement is quite good, if one takes into account that the predictions have no adjustable parameter and are strictly determined by the choice of the initial condition. However, especially the plot in lin-lin scale (panel (d) in Fig. 5) reveals that our theory is unable to reproduce the double bump obtained in numerical simulations. The presence of this bumpy feature is confirmed by simulating the Vlasov equation (4) (see Fig. 6) [20]. The double bump in momentum distribution is the result of the presence of two sliding resonances (the two vortices in the lower right panel), for which an explanation that takes into account the specific dynamical properties of the model is necessary [16,20].

Quasi-stationary states have been demonstrated to be robust to both the application of and external bath [21] and to the addition of a small nearest neighbor interaction [22]. The Vlasov equation is exact in the $N \rightarrow \infty$ limit, and people have tried to address the question of finite N corrections. In this respects the most interesting progress is registered in papers by Bouchet and Dauxois [23] and Chavanis [24]. For the sake of completeness, it should be mentioned that a different approach, based on Tsallis statistics, has been proposed to describe quasi-

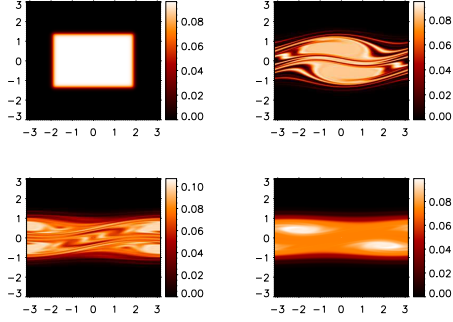


Fig. 6. (color online) Time evolution of the single-particle distribution function according to the Vlasov equation (4) for a rectangular “water-bag” initial state with $\mathcal{E} = 0.69$ and $m_0 = 0.5$.

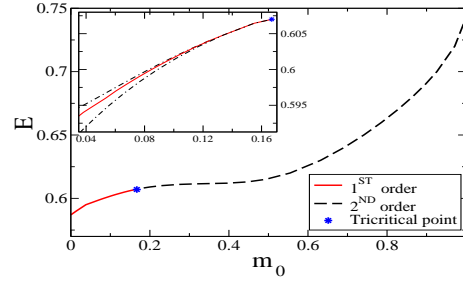


Fig. 7. (color online) Theoretical phase diagram on the control parameter plane (m_0, \mathcal{E}) : second order phase transition line (dashed); first order phase transition line (full); tricritical point (full dot). Inset: magnification of the first order phase transition region and limits of the metastability region (dash-dotted).

stationary states [25]. Recently, these authors have concentrated their attention on the behaviour of correlations in the single particle dynamics, that can give rise to non Gaussian distributions for sums of variables (generalized central limit theorems).

4 Nonequilibrium tricritical point

The maximization of Lynden-Bell entropy reserves another surprise. Since this variational problem introduces another control parameter besides energy, the magnetization m_0 of the initial state, one obtains a phase transition at an energy that depends on m_0 . The transition energy coincides with that given by Boltzmann entropy (to which Lynden-Bell’s entropy reduces in the diluted limit $\bar{f} \ll f_0$) only for $m_0 = 1$. Not only, below $m_0 = 0.61$ the transition becomes first order. The full phase diagram is plotted in Fig. 7. A *nonequilibrium tricritical point* is present in the phase diagram. The specific heat is negative along all the transition line and a temperature jump appears when the transition change to first order.

Numerical simulations confirm this extremely interesting theoretical finding [26]. For instance, we plot in

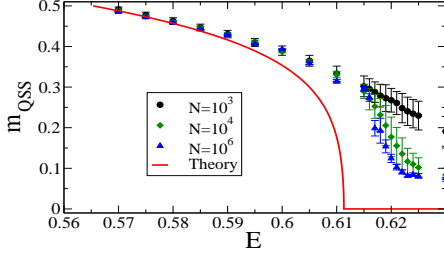


Fig. 8. (color online) m_{QSS} as a function of \mathcal{E} for $m_0 = 0.30$ where the phase transition is second order. The full line is the theoretical prediction and the points are simulations of the HMF model for which the number of initial realizations is 10^5 ($N = 10^3$), 10^4 ($N = 10^4$), 10^2 ($N = 10^6$) and the averaging time $20 < t < 100$.

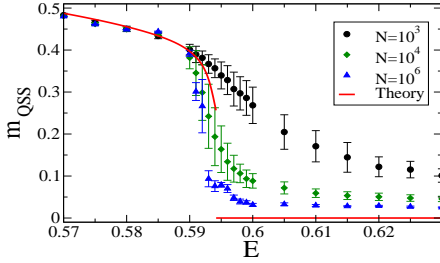


Fig. 9. (color online) m_{QSS} as a function of \mathcal{E} for $m_0 = 0.05$ where the phase transition is first order. The results are plotted as in Fig. 8.

Figs. 8,9 the order parameter m_{QSS} as a function of energy density at fixed m_0 , finding signature of a second order (Fig. 8) or first order (Fig. 9) phase transition. As previously explained, these are “short-time” phase transitions, at variance with the “long-time” phase transitions of equilibrium statistical mechanics. Hence, in order to reveal them numerically, one has to average over a short initial time and take many initial instances.

5 Broken ergodicity

After this excursion in nonequilibrium, let us come back to equilibrium properties. The XY model (2), for some specific choice of antiferromagnetic $J < 0$ and ferromagnetic $K > 0$ couplings has energy density values where regions with different magnetization m are disconnected if energy is fixed (as shown in Fig. 1) [27]. An example is given in Fig. 10, where we show two different situations. In panel a) the “standard” ergodicity breaking associated with a phase transition is revealed by successive magnetization switches between local entropy maxima: the number of particles is small ($N = 20$) such that the entropy barrier (see inset) is not insurmountable. In panel b) we display the new type of *microcanonical broken ergodicity* first dis-

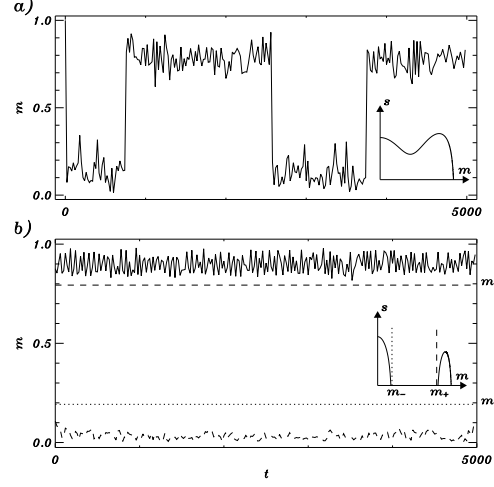


Fig. 10. Time evolution of the magnetization m of model (2) for: a) $\mathcal{E} = 0.1$, $J = -1$ and $K = 8$; b) $\mathcal{E} = 0.1077$, $J = -1$ and $K = 3$, obtained integrating the equations of motion derived from Hamiltonian (2) with $N = 20$. In panel a) magnetization switches between the two most probable values (see the inset for the dependence of entropy on m). In panel b), two different initial conditions are plotted simultaneously, corresponding to two different values of the initial magnetization, $m_0 = 0.1$ and $m_0 = 0.98$. The inset shows the entropy, which now vanishes in the interval $[m_-, m_+]$. Here $m_- \simeq 0.192$ and $m_+ \simeq 0.794$, which are shown to bound from above (dotted line) and from below (dashed line) the magnetization of the two initial conditions.

cussed in Refs. [6,28]: now magnetization cannot switch because there is a gap $[m_-, m_+]$ with no macrostates.

6 Application to the free electron laser

Free-Electron Lasers (FELs) are coherent and tunable radiation sources, which differ from conventional lasers because they use a relativistic electron beam as their lasing medium, hence the term “free-electron”. The physical mechanism responsible for light emission and amplification is the interaction between the relativistic electron beam, a magnetostatic periodic field generated in the undulator and an optical wave co-propagating with the electrons. Due to the presence of the magnetic field, electrons are forced to follow oscillating (typically sinusoidal) trajectories and emit synchrotron radiation. This *spontaneous emission* is then amplified along the undulator until the laser effect is reached. Among the different schemes, single-pass high-gain FELs are currently attracting a growing interest. Basic features of the system dynamics are successfully captured by a simple Hamiltonian model introduced by Colson and Bonifacio [29]

$$\begin{aligned} \frac{d\theta_j}{d\bar{z}} &= p_j \\ \frac{dp_j}{d\bar{z}} &= -\mathbf{A}e^{i\theta_j} - \mathbf{A}^*e^{-i\theta_j} \end{aligned}$$

$$\frac{d\mathbf{A}}{d\bar{z}} = i\delta\mathbf{A} + \frac{1}{N} \sum_j e^{-i\theta_j}, \quad (7)$$

where $\bar{z} = 2k_w \rho z \gamma_r^2 / \langle \gamma \rangle_0^2$ is the rescaled longitudinal coordinate, which plays the role of time. Here, $\rho = \gamma_r^{-1} (\frac{a_w \omega_p}{4ck_w})^{2/3}$ is the so-called Pierce parameter, $\langle \gamma \rangle_0$ the mean energy of the electrons at the undulator's entrance, $k_w = 2\pi/\lambda_w$ the wave number of the undulator, $\omega_p = (4\pi e^2 n/m)^{1/2}$ the plasma frequency, c the speed of light, n the total electron number density, e and m respectively the charge and mass of one electron. Furthermore, $a_w = eB_w/(k_w mc^2)$, where B_w is the rms peak undulator field. Here $\gamma_r = (\lambda_w(1 + a_w^2)/2\lambda)^{1/2}$ is the resonant energy, λ_w and λ being respectively the period of the undulator and the wavelength of the radiation field. Introducing the wavenumber k of the FEL radiation, the two canonically conjugated variables are (θ, p) , defined as $\theta = (k + k_w)z - 2\delta \rho k_w z \gamma_r^2 / \langle \gamma \rangle_0^2$ and $p = (\gamma - \langle \gamma \rangle_0) / (\rho \langle \gamma \rangle_0)$. θ corresponds to the phase of the electrons with respect to the ponderomotive wave. The complex amplitude $\mathbf{A} = A_x + iA_y$ represents the scaled field, transversal to z . Finally, the detuning parameter is given by $\delta = (\langle \gamma \rangle_0^2 - \gamma_r^2) / (2\rho \gamma_r^2)$, and measures the average relative deviation from the resonance condition. This succinct, but detailed, description of the model should transmit the idea that, by adjusting model parameters, one can really simulate realistic experimental situations.

It can be easily checked that model (7) can be derived from the Hamiltonian

$$H_{FEL} = \sum_{j=1}^N \frac{p_j^2}{2} - N\delta I + 2\sqrt{I} \sum_{j=1}^N \sin(\theta_j - \varphi), \quad (8)$$

where N is the number of electrons and the intensity I and the phase φ of the wave are related to $\mathbf{A} = A_x + iA_y = \sqrt{I} e^{-i\varphi}$. In addition to the energy, the total momentum $P = \sum_j p_j + N\mathbf{A}\mathbf{A}^*$ is also a conserved quantity.

It should also be mentioned that, remarkably, this simplified formulation applies to other physical systems, provided an identification of the variables involved is performed. As an example, consider the electron beam-plasma instability. When a weak electron beam is injected into a thermal plasma, electrostatic modes at the plasma frequency (Langmuir modes) are destabilized. The interaction of the Langmuir waves and the electrons constituting the beam can be studied in the framework of a self-consistent Hamiltonian picture [31], formally equivalent to the one in [29]. In a recent paper [32] we have established a bridge between these two areas of investigation and exploited the connection to derive a reduced Hamiltonian model to characterize the saturated dynamics of the laser.

There are many similarities between model (8) and the HMF model (3), and indeed the canonical free energy of one model can be exactly mapped onto the other [30]. While in the HMF model particles interact directly, in the FEL dynamics electrons interact only through the field \mathbf{A} , whose dynamics depend in turn on those of the electrons. Therefore, already on this basis one could expect

similarities in the behaviours of the two models. Indeed, similarly to the HMF model, Hamiltonian (8) presents a standard second order phase transition of the mean field type. As for the HMF, FEL dynamics is well represented in the $N \rightarrow \infty$ limit by the following Vlasov equation

$$\begin{aligned} \frac{\partial f}{\partial \bar{z}} &= -p \frac{\partial f}{\partial \theta} + 2(A_x \cos \theta - A_y \sin \theta) \frac{\partial f}{\partial p}, \\ \frac{\partial A_x}{\partial \bar{z}} &= -\delta A_y + \frac{1}{2\pi} \int f \cos \theta d\theta dp, \\ \frac{\partial A_y}{\partial \bar{z}} &= \delta A_x - \frac{1}{2\pi} \int f \sin \theta d\theta dp. \end{aligned} \quad (9)$$

Hence, one can similarly expect the existence of quasi-stationary states [15]. A direct simulation of Eqs. (7) is shown in Fig. 11 for $N = 10^4$ electrons. Initially, the electrons are uniformly distributed in the θ interval $[-\pi, \pi]$ and their momentum is also uniformly spread in $[-\Delta p, \Delta p]$ in a “water-bag” distribution: this initial state has a physical meaning, because it is very close to the state in which, experimentally, the electrons are injected into the undulator. The laser intensity I is initially set to a small value, in order to switch on the instability, whose initial growth is exponential. On a short time, the intensity reaches a saturation level and performs wide oscillations around it, but these oscillations dump with time, and a well defined asymptotic intensity is reached. This process is the equivalent of Lynden-Bell’s “violent relaxation”. The N -dependence of the saturation level is shown in the inset, where three different values of N are considered. For the smaller value, $N = 100$ (curve 3), the saturated intensity is larger than for higher N values. When N increases the system remains trapped in the quasi-stationary state for a longer and longer time. The second relaxation to the larger intensity value corresponds to the relaxation to Boltzmann-Gibbs equilibrium. This latter relaxation has no experimental relevance for free electron lasers, because it would take place for enormous undulator lengths. A similar behavior would be observed for the “bunching parameter” $b = |\sum_n \exp(i\theta_n)|/N$, which is the equivalent of the magnetization m of the HMF model.

The distribution $\bar{f}_{QSS}(\theta, p)$ in the quasi-stationary state can be obtained by maximizing Lynden-Bell entropy (5), keeping energy and momentum P fixed. The result of this maximization procedure is very similar to that of the HMF

$$\bar{f}_{QSS}(\theta, p) = \frac{f_0}{e^{\beta(p^2/2 + 2A_{QSS} \sin \theta) + \lambda p + \alpha} + 1}, \quad (10)$$

with

$$A_{QSS} = \sqrt{I_{QSS}} = \frac{\beta}{\beta\delta - \lambda} \int dp d\theta \sin \theta \bar{f}_{QSS}(\theta, p), \quad (11)$$

and β , λ and α are the usual Lagrange multipliers, whose value is determined by the initial condition.

The dependence of both the intensity and the bunching parameter in the quasi-stationary state on the detuning parameter δ for an initially homogeneous state ($\Delta\theta = \pi$) with zero momentum dispersion $\Delta p = 0$ is shown in Fig. (12).

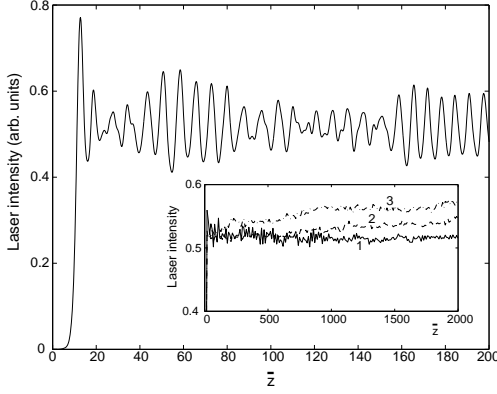


Fig. 11. Typical evolution of the radiation intensity of a free electron laser using Eqs. (7); the detuning δ is set to 0, the energy per electron $H/N = 0.2$ and $N = 10^4$ electrons are simulated. The inset presents averaged simulations on longer times for different values of N : $5 \cdot 10^3$ (curve 1), 400 (curve 2) and 100 (curve 3).

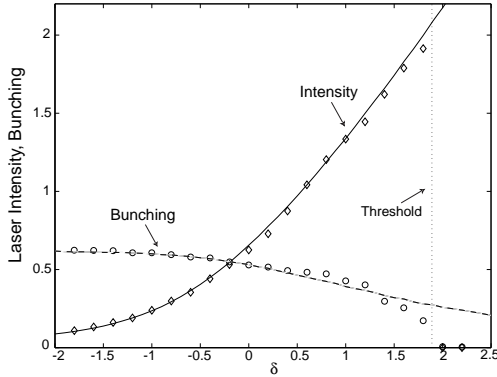


Fig. 12. Laser intensity I_{QSS} and bunching parameter b_{QSS} in the quasi-stationary state as a function of detuning δ : theoretical prediction (solid and dashed lines, respectively) and simulations (symbols). The dotted vertical line, $\delta = \delta_c \simeq 1.9$, represents the transition from the low to the high-gain regime.

If FEL's Hamiltonian is equivalent to HMF, one might wonder if situations exist which produce more complex phase diagrams and dynamical evolutions. Indeed, in the regime where the beam current and the emittance is small, FEL's dynamics is better described by a model where many planar waves interact with the beam

$$\begin{aligned} \frac{d\theta_j}{d\bar{z}} &= p_j \\ \frac{dp_j}{d\bar{z}} &= - \sum_h F_h (\mathbf{A}_h e^{ih\theta_j} - \mathbf{A}_h^* e^{-ih\theta_j}) \\ \frac{d\mathbf{A}_h}{d\bar{z}} &= \frac{F_h}{N} \sum_j e^{-ih\theta_j}, \end{aligned} \quad (12)$$

where the complex amplitudes $\mathbf{A}_h = A_h^x + iA_h^y$ represent the scaled field, transversal to \bar{z} , and the coupling pa-

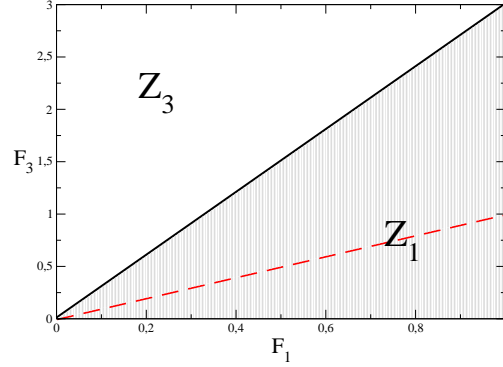


Fig. 13. (color online) Phase diagram in the (F_1, F_3) parameter space for the two-wave model (12), corresponding to a FEL with an initial cold homogeneous beam. Lynden-Bell's theory predicts a transition from a region Z_1 (shaded) dominated by the first wave to one, Z_3 , dominated by its odd harmonic. Above the dashed line the short time growth rate of $|\mathbf{A}_3|$ is predicted to be larger than that of $|\mathbf{A}_1|$ by a linear theory

rameters F_h depend on the experimental setup. We have analysed in some detail [33] only the case with two odd harmonics $h = 1, 3$, performing the same analysis of the quasi-stationary states as for Eqs. (7). The initial condition is again a homogeneous almost monochromatic beam, but now there are two “order parameters”, $|\mathbf{A}_1|$ and $|\mathbf{A}_3|$, with the corresponding bunchings $b_1 = |\sum_j \exp(-i\theta_j)|/N$ and $b_3 = |\sum_j \exp(-i3\theta_j)|/N$. In region Z_1 (shaded) of Fig. 13 the quasi-stationary state is dominated by the first wave: hence $|\mathbf{A}_1| > 0$ and $|\mathbf{A}_3| = 0$. On the contrary, in region Z_3 , $|\mathbf{A}_3| > 0$ and $|\mathbf{A}_1| = 0$. The full line corresponds to a nonequilibrium phase transition of the first order.

However, a linear analysis show that in the region between the dashed line and the transition line to Z_3 (inside the Z_1 region) the growth rate of $|\mathbf{A}_3|$ is larger than that of $|\mathbf{A}_1| = 0$. Therefore, at short time the growth of $|\mathbf{A}_3|$ is expected to be faster and the initial evolution of the FEL is dominated by the first odd harmonic. However, this is not the maximal Lynden-Bell's entropy state, and on a later time, the system is finally going to be dominated by the first wave. This is indeed what happens, as shown in Fig. 14.

7 Conclusions and perspectives

We have discussed both equilibrium and nonequilibrium properties of systems with long range interactions with reference to mean-field models. Most of these features should extend to cases where forces weakly decay [1,30], but this problem remains to be seriously investigated. In this perspective, the general classification of phase transitions obtained in Ref. [34] could be extremely useful.

The domain of application of these ideas is vast and the perspective to perform key experiments in the near future is realistic. We have discussed in some detail in Sect. 6 a realistic model of the free electron laser. However, we can foresee applications to all systems where particles interact

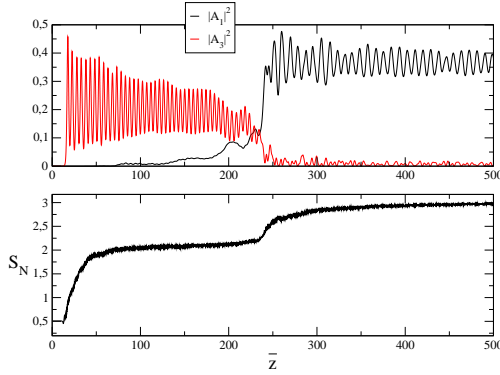


Fig. 14. (color online) Upper panel: Evolution of the intensities $|A_1|^2$ and $|A_3|^2$ showing an initial growth of the first odd harmonic followed by the final relaxation to the maximal Lynden-Bell's entropy state dominated by the first wave. Lower panel: time evolution of Lynden-Bell's entropy

with waves in a self-consistent way. As an example, let us mention collective atomic recoil lasers, where ultracold atoms interact with the optical modes of the cavity, determining collective effects and first and second order phase transitions [35].

Another domain where experimental applications are envisageable is that of layered spin structures, where dipolar interactions dominate over Heisenberg exchange [36]. In this case, a mean-field term of the Hamiltonian is shown to depend on the shape of the sample, determining the presence or absence of phase transitions [37].

Most of my knowledge of the physics of systems with long-range interactions has been shaped by J. Barré, F. Bouchet, P.H. Chavanis, T. Dauxois, D. Fanelli D.H.E. Gross, D. Mukamel, Y.Y. Yamaguchi. I also thank all the coauthors of my papers on this subject, with whom I have entertained endless discussions. This work is funded by the PRIN05 grant *Dynamics and thermodynamics of systems with long-range interactions*.

References

1. T. Dauxois, S. Ruffo, E. Arimondo and M. Wilkens (Eds.) *Dynamics and thermodynamics of systems with long-range interactions* (Springer, Berlin 2001).
2. L. Onsager, *Il Nuovo Cimento* (Suppl.) **6**, (1949) 279.
3. V. A. Antonov, *Leningrad Univ.* **7**, (1962) 135 [translation in *IAU Symposium* **113**, (1995) 525]; D. Lynden-Bell, R. Wood, *Mon. Not. R. Astr. Soc.* **138**, (1968) 495; P. Hertel and W. Thirring, *Annals of Physics*, **63**, (1971) 520.
4. A. Campa, S. Ruffo and H. Touchette, *Physica A*, **385**, (2007) 233.
5. J. Barré, D. Mukamel and S. Ruffo, *Phys. Rev. Lett.*, **87**, (2001) 030601.
6. D. Mukamel, S. Ruffo and N. Schreiber, *Phys. Rev. Lett.* **95**, (2005) 240604.
7. M. K. H. Kiessling and J.L. Lebowitz, *Lett. Math. Phys.* **42**, (1997) 43 and refs. therein; R. S. Ellis, K. Haven and B. Turkington, *J. Stat. Phys.*, **101**, (2000) 999.
8. I. Ispolatov and E.G.D. Cohen, *Phys. A*, **295**, (2001) 475.
9. J. de Luca, A.J. Lichtenberg and S. Ruffo, *Phys. Rev. E*, **60**, (1999) 3781.
10. Y.Y. Yamaguchi, J. Barré, F. Bouchet, T. Dauxois, S. Ruffo, *Physica A*, **337**, (2004) 36.
11. P.H. Chavanis, Ph. D Thesis, ENS Lyon (1996); P.H. Chavanis, J. Sommeria and R. Robert, *Astroph. J.*, **471**, (1996) 385.
12. F. Hohl and J.W. Campbell, *Collective motion of a one-dimensional self-gravitating system*, NASA Technical Note TN D-5540, November (1969).
13. T. Yamashiro, N. Gouda and M. Sakagami, *Prog. Theor. Phys.*, **88** (1992) 269.
14. M. Antoni and S. Ruffo, *Phys. Rev. E* **52**, (1995) 2361.
15. J. Barré, T. Dauxois, G. De Ninno, D. Fanelli and S. Ruffo, *Phys. Rev. E*, **69**, (2004) 045501.
16. P.H. Chavanis, *Eur. Phys. J. B* **53**, (2006) 487; A. Antoniazzi, D. Fanelli, J. Barré, P.-H. Chavanis, T. Dauxois and S. Ruffo, *Phys. Rev. E*, **75**, (2007) 011112.
17. P. de Buyl, D. Mukamel and S. Ruffo, in *Unsolved Problems of Noise and Fluctuations*, AIP Conference Proceedings **800**, (2005) 533.
18. P.H. Chavanis, J. Vatteville and F. Bouchet, *Eur. Phys. J. B*, **46**, (2005) 61.
19. W. Braun and K. Hepp, *Comm. Math. Phys.* **56**, (1977) 101.
20. A. Antoniazzi, F. Califano, D. Fanelli and S. Ruffo, *Phys. Rev. Lett.*, **98**, (2007) 150602.
21. F. Baldovin and E. Orlandini, *Phys. Rev. Lett.*, **96**, (2006) 240602; F. Baldovin and E. Orlandini, *Phys. Rev. Lett.*, **97**, (2006) 100601.
22. A. Campa, D. Mukamel, A. Giansanti and S. Ruffo, *Phys. A*, **365**, (2006) 120.
23. F. Bouchet and T. Dauxois, *Phys. Rev. E*, **72**, (2005) 045103(R).
24. P. H. Chavanis, *Phys. A*, **361**, (2006) 55; *ibid.* **361**, (2006) 81; doi:10.1016/j.physa.2007.10.026, doi:10.1016/j.physa.2007.10.034.
25. V. Latora, A. Rapisarda and C. Tsallis, *Phys. Rev. E*, **64**, (2001) 056134; A. Pluchino, A. Rapisarda and C. Tsallis, *cond-mat.stat-mech/0706.4021v2*.
26. A. Antoniazzi, D. Fanelli, S. Ruffo and Y.Y. Yamaguchi, *Phys. Rev. Lett.*, **99**, (2007) 040601.
27. F. Bouchet, T. Dauxois, D. Mukamel and S. Ruffo, *Phase space gaps and ergodicity breaking in systems with long range interactions*, arXiv:0711.0268.
28. F. Borgonovi, G.L. Celardo, M. Maianti and E. Pedersoli, *J. Stat. Phys.*, **116**, (2004) 1435.
29. W. B. Colson, *Phys. Lett. A*, **59**, (1976) 187; R. Bonifacio et al., *Opt. Comm.*, **50**, (1984), 373.
30. J. Barré, F. Bouchet, T. Dauxois and S. Ruffo, *J. Stat. Phys.* **119**, (2005) 677.
31. Y. Elskens and D.F. Escande, *Microscopic Dynamics of Plasmas and Chaos*, (IoP Publishing, Bristol 2003).
32. A. Antoniazzi, G. De Ninno, D. Fanelli, A. Guarino and S. Ruffo, *J. Phys.: Conf. Ser.*, **7**, (2005) 143.
33. A. Antoniazzi, R. S. Johal, D. Fanelli and S. Ruffo, *Comm. Nonlin. Sci. Num. Simul.*, **13**, (2008) 2.
34. J. Barré and F. Bouchet, *J. Stat. Phys.* **118**, (2005) 1073.
35. C. von Cube et al., *Phys. Rev. Lett.*, **93**, (2004) 083601; C. von Cube et al., *Fortschr. Phys.*, **54**, (2006) 726.
36. L.Q. English, M. Sato and A. J. Sievers, *Phys. Rev. B*, **67**, (2003) 024403.
37. A. Campa, R. Khomeriki, D. Mukamel and S. Ruffo, *Phys. Rev. B*, **76**, (2007) 064415.

